The Effect of Ignition Procedure on Flashback of Hydrogen-Enriched Flames

Tarik Yahou, Thierry Schuller, James R Dawson

▶ **To cite this version:**

Tarik Yahou, Thierry Schuller, James R Dawson. The Effect of Ignition Procedure on Flashback of Hydrogen-Enriched Flames. Journal of Engineering for Gas Turbines and Power, 2024, 146 (1), 10.1115/GT2023-101785 . hal-04584108

HAL Id: hal-04584108
https://hal.science/hal-04584108v1

Submitted on 22 May 2024

HAL is a multi-disciplinary open access archive for the deposit and dissemination of scientific research documents, whether they are published or not. The documents may come from teaching and research institutions in France or abroad, or from public or private research centers.

L'archive ouverte pluridisciplinaire **HAL**, est destinée au dépôt et à la diffusion de documents scientifiques de niveau recherche, publiés ou non, émanant des établissements d'enseignement et de recherche français ou étrangers, des laboratoires publics ou privés.

THE EFFECT OF IGNITION PROCEDURE ON FLASHBACK OF HYDROGEN-ENRICHED FLAMES

Tarik Yahou [a,b*], **Thierry Schuller** [b] **and James R. Dawson** [a]

[a]Department of Energy and Process Engineering. Norwegian University of Science and Technology
Trondheim, Norway

[b]Institut de Mécanique des Fluides de Toulouse, IMFT. Université de Toulouse, CNRS
Toulouse, France

ABSTRACT

The impact of different ignition sequences on the ignition dynamics of CH_4-H_2 flames in a bluff body burner is investigated at atmospheric conditions. Experiments are performed over a wide range of operating conditions covering pure methane injection (PH0) to pure hydrogen injection (PH100). A perforated plate of total porosity $\sigma = 0.17$ is positioned at the outlet of the combustion chamber to increase the chamber back pressure and trigger transient flashback during ignition. Time-series of pressure, OH^* chemiluminescence and OH-PLIF images of the propagating flame branch are recorded simultaneously to characterize the ignition process. Two ignition procedures are investigated. For ignition procedure A, designated as an early ignition procedure, the spark is initiated before fuel injection. For ignition procedure B, designated as a late ignition, the spark is only activated after the fuel injection. The impact of the fuel air mixing on the final stabilization state is investigated by changing the fuel delivery time (dt) before the initial spark. Three different time delays are considered $dt = 1$, 3 and 5 s. The final state of the flame is found to be highly sensitive to the selected ignition procedure and increasing dt favors the occurrence of flashback. At constant power, the magnitude of the pressure peak is driven by a competition between the fuel mass flow rate at the moment of ignition and the high reactivity of hydrogen which shifts the flammability limit towards lower equivalence ratios, hence generating a lower reaction rate. For procedure A, the peak of the chamber over pressure shows a non-monotonic growth for increasing levels of H2 in the fuel blend, while it linearly increases for procedure B. Experiments are then conducted at a fixed injection flow velocity $U_b = 5\ m.s^{-1}$ and fixed laminar burning velocity $S_l^0 = 0.25\ m.s^{-1}$ by varying the level of hydrogen enrichment. For procedure A, the over pressure amplitude decreases with increasing the hydrogen enrichment leading to a soft ignition for all CH_4-H_2 blends. Under ignition procedure B, the amplitude of the over pressure reached during ignition is found to be relatively unaffected by the hydrogen concentration, but the flame stabilization mode shows a strong dependence to both the level of H_2-enrichment and fuel delivery time dt. OH^* as well as OH-PLIF images reveal that the trajectory of the flame leading point changes as dt increases. The different dynamics of the flame leading points is likely to be the cause the different types of stabilization modes observed.

1 Introduction

In the drive to reduce carbon dioxide footprint, carbon free fuels such as green hydrogen offers a promising alternative to achieve a smooth transition towards net zero emissions [1, 2]. Nevertheless, adding increasingly higher amounts of hydrogen to conventional hydrocarbon fuels raises many challenges that need to be addressed [3, 4]. Due to its high reactivity, hydrogen enrichment considerably modifies the fundamental combustion process [4, 5], which may compromise compliance with safety standards.

*Corresponding author. E-mail: tarik.yahou@ntnu.no

On this matter, one of the major issues driving the design of any aero-engine and/or power plant combustor is to guarantee a safe and reliable ignition sequence for a wide range of H_2-content. Forced ignition has been extensively studied over the last hundred years starting from Neuman's groundbreaking work [6]. It is commonly accepted that the ignition sequence can be decomposed into a series of successive steps. A typical ignition starts from a plasma leading to a flame kernel which develops to a fully turbulent propagating flame to reach a final stabilization state [7]. A large effort has been devoted to the understanding of the mechanisms controlling flame initiation and the determination of minimum ignition energies for various fuels [8, 9, 10]. These studies demonstrated the stochastic nature of the ignition and its dependence to the local flow properties accounting for complex flow topology as well as its variability during ignition [11]. Recently, research has been concerned with the transition from the initial flame kernel to fully established flame in both single sector [12, 13] and annular combustors with multiple injectors [14, 15]. It has been shown that a successful flame growth is governed by the direction of the instantaneous velocity and the local strain rate in the vicinity of the spark. Recent direct numerical simulations of ignition in high-speed flows above a backward step combustor [16], have shown that the ability of a flame to propagate into different regions of the flow is essentially governed by the local strain rate in the shear regions, leading to flame quenching when the strain rate exceeds a critical extinction rate.

Due to the high reactivity of hydrogen compared to hydrocarbon fuels, new questions arise for safe ignition of burners powered by hydrogen. Only few studies have been dedicated to assessing the consequences of violent ignition. For instance, due to the volumetric expansion of the burned gases, ignition can generate, a strong acoustic fluctuation which may perturb the flow at the injector outlet and lead to flame flashback immediately after ignition of fully premixed systems [17]. This violent phenomena have also been observed in single and multiple spray-injector configurations in [18, 19]. The flame is in these cases entrained by the strong transient flow perturbation caused by the sudden rise in pressure with a transient flow blockage at the burner outlet that alters the flame shape switching from anchored state inside the injector to a lifted flame.

These interactions between ignition and flashback have further been investigated for hydrogen enriched mixtures in [17]. It was demonstrated that increasing the hydrogen content in the fuel blend, not only leads to a significant amplification of the pressure impulse, but also considerably modifies the final stabilization state of the flame. Three different scenarios have been identified: no flashback, transient flashback and permanent flashback. Interestingly, experiments at fixed injection flow velocity and constant laminar burning velocity have shown that although the mean flow conditions and over pressures are kept constant, the stabilization mode directly depends on the H_2-content in the fuel blend. It was also shown that the synchronization between the pressure peak and the maximum of the heat release rate is a sufficient condition to trigger flashback [17].

Regardless, these results were obtained for a specific ignition sequence where the chamber was entirely filled with combustible mixture before ignition. In a real engine, sparks would eventually be initiated before fuel injection. This work aims to investigate the impact of initial pre-fuelling time on the ignition dynamics of a CH_4-H_2-air fueled burner. To do this, the ignition sequence is varied by changing the time delay dt between the fuel injection and initial spark. Ignition experiments are performed over a wide range of operating conditions covering pure methane injection (PH0) to pure hydrogen injection (PH100). First, a comparison of the stabilization maps showing the final state of the flame after ignition is provided. This is followed by a detailed analysis of the pressure time traces for the different ignition sequences considered in this study when the thermal power is kept constant. Finally, the effect of the selected ignition procedure on the final stabilization mode is investigated for a fixed bulk flow velocity and constant laminar burning velocity by varying the hydrogen concentration in the fuel blend.

2 Experimental setup and methods

2.1 Burner setup

Figure 1 shows a schematic of the experimental setup, which is a single sector rig already used in [17]. Alicat flow controllers (MFC), placed about 4 m upstream of the burner inlet, provide independent control and time traceability of the CH_4, H_2 and air mass flow rates through the injectors. The MFCs are accurate to 0.8% of the reading and $\pm 0.2\%$ of the full scale. The combustible mixture is injected through the bottom plenum and flows to the chamber through a pipe of inner diameter $d_p = 30$ mm. The flames are stabilized above a conical bluff body of a diameter $d_b = 16$ mm, centered on a plenum attached rod of diameter $d_r = 6$ mm. The flames are confined inside a cylindrical quartz combustion chamber of inner diameter $d_{cc} = 60$ mm and a total length $l_{cc} = 150$ mm. A perforated plate of a total porosity $\sigma = 0.17$ is placed at the combustor exit to increase the chamber back pressure. The plate has 5×5 holes of 5 mm diameter each, evenly distributed in a square pattern with 7 mm spacing. With the plate, the total pressure drop ΔP in the system is increased by 100 Pa at the desired operating conditions. It is important to note that this small increase in the static pressure is sufficient to generate significant over pressures during ignition [17].

2.2 Measurements and diagnostics

Time evolution of the static and the dynamic pressure in the combustion chamber is measured using a Kulite XTM-190LM transducer (± 35 Pa accuracy) placed in a water cooled wave guide, labelled M4 in Fig. 1. This pressure signal is corrected

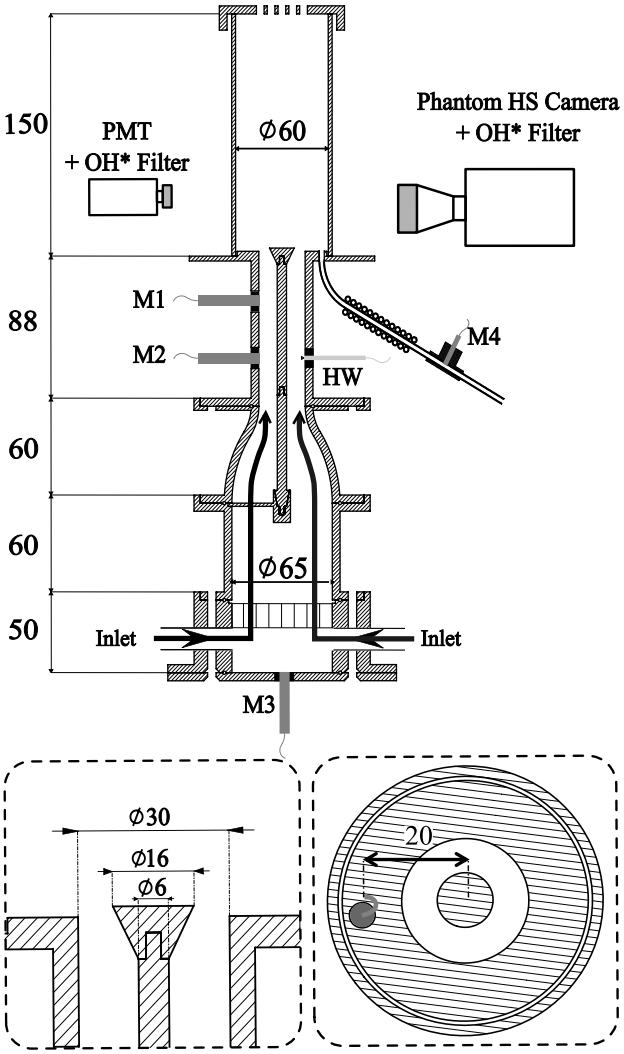

Fig. 1: Sketch of the experimental bench with relevant dimensions in millimeters.

by using the wave guide transfer function measured separately in an acoustically forced pipe. For consistency of the measurements, three other pressure sensors labelled M1 to M3 in Fig. 1 were also recorded simultaneously. Time resolved images of the propagating flame as well as the global OH* chemiluminescence are gathered simultaneously with a Phantom V2012 high-speed intensified camera (LaVision IRO) with a Cerco 2178 UV lens 100F/2.8 and a Hamamatsu H11902-13 photomultiplier module, with a spectral response of 185 nm to 700 nm, respectively. Both sensors were fitted with a UV narrow bandpass filter centered on the OH* emission peak intensity 310 ± 10 nm. It is well established that under perfectly premixed conditions, OH* emission is an appropriate approximation for heat release rate. Pressure and OH* signals are sampled at a rate of 52.5 kHz and digitized using

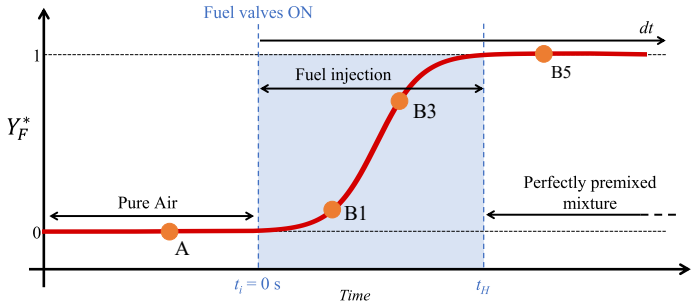

Fig. 2: Schematic representation of the different ignition procedures considered in this study.

a 24-bit NI-9234 DAQ while the camera is sampled at 10 kHz. A planar view (aligned with the central axis) of the traveling flame branch is isolated using high speed OH-PLIF system shooting at 10 kHz. A 100 W Edgewave laser is used to pump a Sirah Credo-Dye-N laser of 3 W total output power. The wavelength was tuned to match the absorption peak of the OH* radicals at 283 nm.

2.3 Operating conditions

Experiments consider a wide range of CH_4-H_2-air mixtures, including pure methane and pure hydrogen injection conditions. The H_2-contents in the fuel blend is defined in terms of power fraction $\mathrm{PH} = \mathcal{P}_{H_2} / (\mathcal{P}_{H_2} + \mathcal{P}_{CH_4})$ originating from hydrogen combustion. Gases are injected into the bottom plenum at room temperature $T_u = 298$ K. Ignition experiments are only carried out in lean operating conditions for equivalence ratios $0.3 \leq \phi \leq 0.8$ at constant bulk flow velocity $U_b = 5$ m.s^{-1} measured in the injector pipe. This corresponds to a total thermal power range $3.5 \leq \mathcal{P} \leq 9.0$ kW. For a fixed value of equivalence ratio ϕ, the total thermal power $\mathcal{P}$ remains constant within $\pm 5\%$ over all the span of fuel blends tested. These conditions correspond to injection Reynolds numbers $Re_{d_h} = 7170$ based on the hydraulic diameter $d_h = d_p - d_b = 14$ mm of the annular injection channel.

2.4 Ignition procedure

The ignition system used in this study is made of an electric spark plug connected to a Danfoss EB14 transformer used to initiate the flame kernel. The igniter is positioned in the outer recirculation zone above the combustor dump plate approximately 20 mm away from the center of the bluff-body. The ignition system delivers 36 mJ mean energy every 20 ms. This energy is two order of magnitude higher than the minimum energy needed to ignite a methane/air mixture at $\phi = 0.7$. To minimize wall temperature effects on the ignition dynamics [20], the burner is cooled down to room temperature after each ignition sequence.

The impact of the pre-fueling time on the ignition dynam-

ics is investigated by controlling the ignition sequence. This is made by changing the time lag dt between fuel injection and the initial spark. This allows the total mass of fuel in the chamber to be varied at ignition as qualitatively represented in Fig. 2. This figure shows the time evolution of the reduced fuel mass fraction $Y_F^* = Y_F/Y_F^\infty$, where Y_F is the instantaneous fuel mass fraction inside the combustion chamber and Y_F^∞ its value at steady operation. The orange circles denote the instants when the first spark is initiated. Two ignition procedures are considered: Procedure A in Fig. 2 designates an early ignition procedure by first sparking and then opening the fuel valve ("spark first, fuel later"). The air flowrate is first fixed at the desired operating condition and then, sparks are repeatedly applied. The fuel valve is opened with a targeted mass flowrate. In this procedure, ignition takes place at the instant when a sufficiently flammable fuel air mixture has reached the near field of the spark. Procedures B, including B1, B3 and B5, in Fig. 2 designate a series of late ignition procedures. The air flow rate is first set to the targeted value and the spark plug is only activated after fuel injection ("fuel first, spark later"). Three different time lags are considered $dt = 1$ s (B1), 3 s (B3) and 5 s (B5). To ensure that ignition occurs at the desired time delay, only five successive sparks corresponding to a sparking time window of 100 ms are produced. In the event of an ignition failure within this time window, the ignition sequence is stopped, the combustion chamber is purged and the procedure is restarted again. For procedure B, the volume of the fuel injected increases when dt increases. Tests revealed that full homogeneity is reached for ignition procedure B5 for a time delay $dt = 5$ s, in which case ignition occurs in a perfectly premixed volume.

3 Results and discussion

3.1 Stability maps

The ignition dynamics is first examined for the range of operating conditions presented in Section 2.3. A minimum of five successive ignition sequences are performed for each point. For the sake of brevity, results are shown only for ignition procedures A, B1 and B3.

The stabilization map for ignition procedure A is presented in Fig. 3. It shows the evolution of the magnitude of pressure peak p_{max} reached during ignition as a function of the mixture equivalence ratio ϕ and the H2 hybridization rate PH. The size and the color of the disks are proportional to p_{max}. Similarly as in [17], the green shaded region delineates the soft ignition points where the flame directly stabilizes on the bluff body. The red shaded region denotes the points where the flame immediately flashes back after ignition. Finally, the orange shaded region shows the transitional points for which the final state of the flame varies from an ignition sequence to another. The bottom left and the upper right regions represent the lean blow off and the flashback limits, respectively. Figure 3 shows that the early ignition procedure A corresponds globally to a safe ignition procedure for which only a few points along the descending red diagonal characterized by high equivalence ratios ($\phi \geq 0.5$) and high H_2-contents (PH $\geq 50\%$) lead to flashback after ignition (red and orange shaded regions in Fig. 3). In addition, the magnitude of the over pressure remains moderate and lies within a range between 2 kPa $\leq p_{max} \leq$ 9 kPa depending on the operating

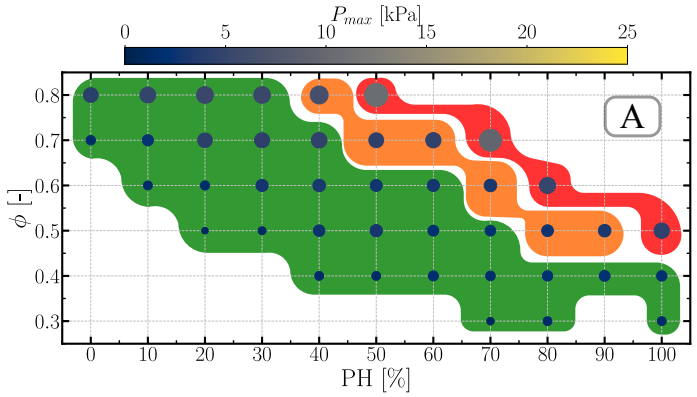

Fig. 3: Stability map for early ignition procedure A.The size and the color of the disks are proportional to p_{max}. The green shaded region delineates the soft ignition zone, the orange one the transient flashback regime and the red one the flashback region.

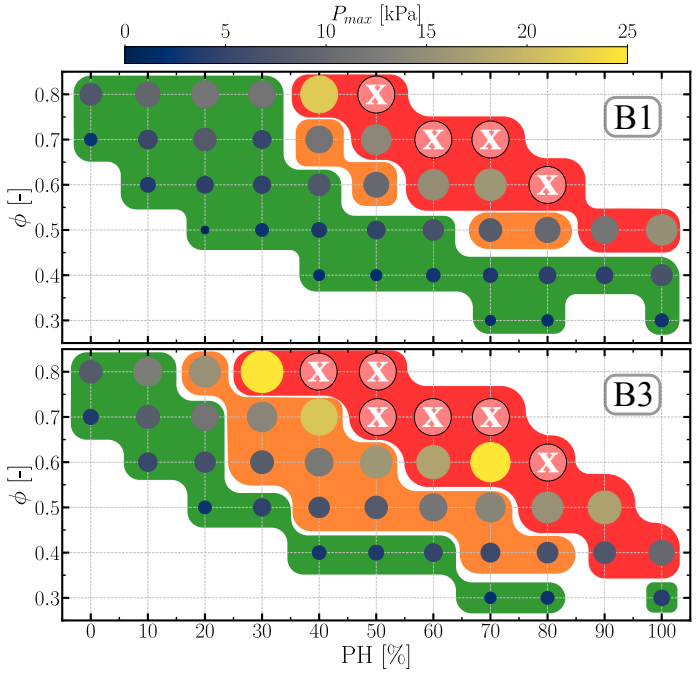

Fig. 4: Stability map for late ignition procedures (B1 in the upper figure and B2 in the lower figure). Red markers with **X** symbols correspond to operating conditions that could not be fully explored. The color code is kept the same as in Fig. 3.

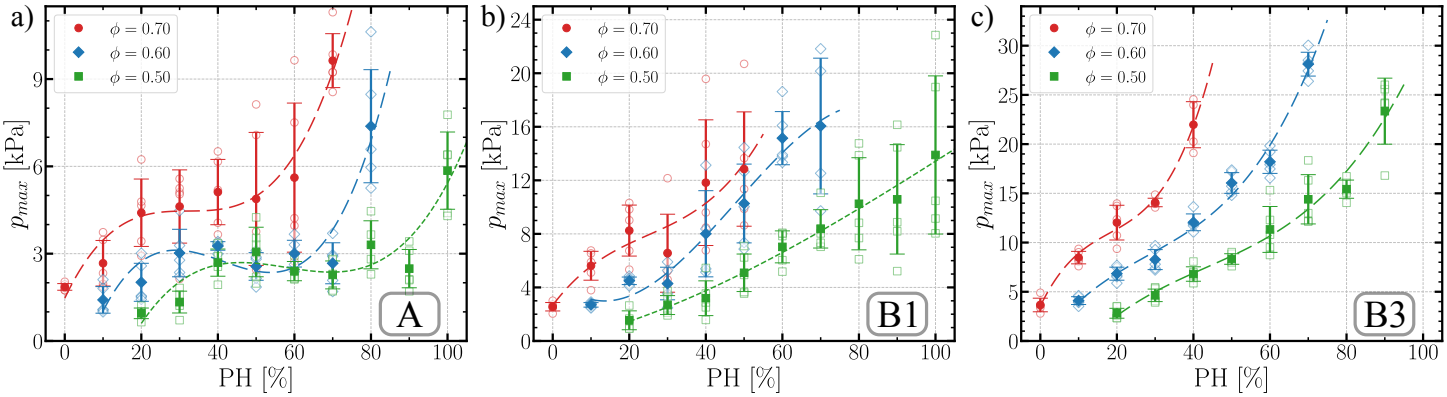

Fig. 5: Measured pressure peak at iso-values of $\phi = 0.5$, 0.6 and 0.7 for ignition procedures (a) A, (b) B1 and (c) B3. Empty markers denote a single sequence, the colored markers indicate the average and the bars the standard deviation.

condition.

The impact of late ignition procedures B is examined in Fig. 4. The upper figure shows the stability map for ignition procedure B1 and the lower figure shows the one corresponding to procedure B3. Red markers with **X** symbols correspond to operating conditions that could not be fully explored due to safety issues associated to pressure overshoot exceeding 30 kPa. For these ignition procedures, the operability range without flashback is drastically reduced as the pre-fueling time delay dt increases. The total number of safe ignition points reduces by one fourth for B1 and one half for B3. Temporary (orange shaded region) and permanent (red) flashbacks become predominant and the flashback limit is significantly shifted toward lower hydrogen concentrations. Despite a relatively low pre-fueling time, experiments show that the safe ignition time window is considerably reduced for both B1 and B3 procedures at high H_2-content. These experiments highlight the substantial impact of the ignition procedure in compromising the safety compliance of next generation of hydrogen-fired gas turbines. Moreover, the magnitude of the pressure perturbation during ignition significantly increases for ignition procedures B. The pressure peak amplitude varies from $p_{max} = 2$ kPa when $\phi = 0.3$ which corresponds to the lowest thermal power ($\mathcal{P} \sim 3.5$ kW) up to $p_{max} = 25$ kPa for the highest thermal power ($\mathcal{P} \sim 9$ kW) at $\phi = 0.8$. These effects are directly related to the total fuel mass inside the combustion chamber (expressed in terms of Y_F^* in Fig. 2) at ignition. For instance, a small increase in the pre-fuelling time dt, results in an increase of the total volume of the ignited fuel inside the combustion chamber, which in turn, leads to an important pressure perturbation, hence promoting flashback. These observations underline the sensitivity of the final state of the flame to small variation in Y_F at ignition instant. Finally, following an iso-value of ϕ, i.e. also a constant power, the impact of hydrogen enrichment on the magnitude of the pressure impulse p_{max} is found to be more important when dt increases. The over pressure is amplified by a factor of 2 between PH0 and PH50 at $\phi = 0.7$ with the ignition procedure A, but exceeds a factor of 5 to 10 for ignition procedures B1 and B3, respectively for the exact same operating conditions. This is further investigated in the next section.

3.2 Analysis

3.2.1 Pressure time-series The amplitude of the pressure peaks is plotted in Fig. 5(a-c) for the different ignition procedures considered in this study. They are plotted following three iso-values of $\phi = 0.5$, 0.6 and 0.7 for increasing H2 concentrations in the fuel blend. When ignition procedure A is used (Fig. 5.a), the peak of the chamber over-pressure p_{max} shows a non-monotonic growth with increasing H2 levels. It first increases for low hydrogen concentrations PH0 $\leq$ PH $\leq$ PH30. Then, it remains relatively constant around $p_{max} \sim 3$ kPa at $\phi = 0.5$ and 0.6 and $p_{max} \sim 5$ kPa at $\phi = 0.7$ for PH30 $\leq$ PH $\leq$ PH60. At higher hydrogen enrichment levels, for PH $\geq$ 60%, it quickly increases again. This trend is counter-intuitive considering the significant increase in the laminar burning velocity S_l^0 as the H_2-content is increased in the fuel blend. The increase of the laminar burning velocity was indeed shown to have a leading impact on the amplitude reached by the pressure during ignition [17]. For ignition procedures B, the peak pressure inside the chamber increases monotonically for increasing levels of H_2 in the fuel in a quasi-linear manner, regardless the pre-fuelling time dt (see Fig. 5.b-c). This behavior is more consistent with the higher reactivity of hydrogen leading to higher flame accelerations as the hydrogen level increases. However, the growth rate of the magnitude p_{max} with respect to PH is found to depend on the selected pre-fuelling time ($dt = 1$ s or 3 s) considering the transient variation of the total fuel mass at ignition. Furthermore, for a fixed mixture composition, the variation of the magnitude of the pressure impulse p_{max} over the different ignition procedures directly depends on the H_2-content in the fuel. The measured

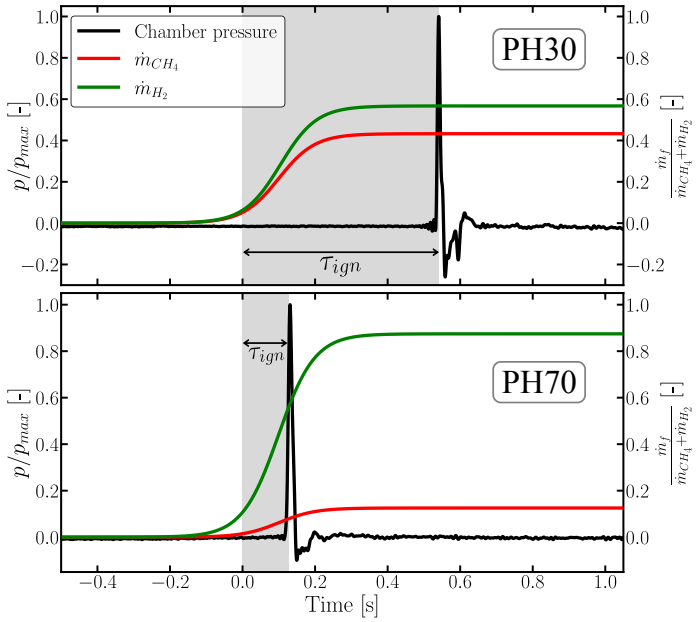

Fig. 6: Times-series of the chamber pressure (black line), CH_4 (red line) and H_2 mass flowrates (green line) during the ignition sequence of PH30 (top figure) and PH70 (bottom figure) at $\phi = 0.6$. The gray region marks the ignition time delay τ_{ign}.

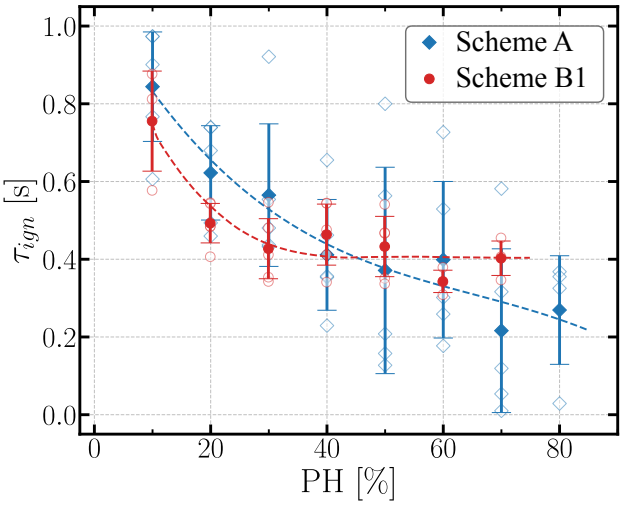

Fig. 7: Ignition time delay τ_{ign} at $\phi = 0.6$ for increasing levels of H_2 for both ignition schemes A (blue) and B1 (red).

pressure peak at PH50 and $\phi = 0.7$ goes from $p_{max} \sim 3$ kPa for ignition procedure A, and exceeds $p_{max} \sim 11$ kPa and ~ 30 kPa for procedures B1 and B2, respectively. For lower hydrogen concentrations, PH ≤ 20, this variation is less pronounced and varies only from $p_{max} \sim 2$ kPa to ~ 2.5 kPa and finally to ~ 3 kPa for ignition procedures A, B1 and B2, respectively at PH0 and $\phi = 0.7$. Under these conditions, the amplitude of the pressure perturbation is less sensitive to variations of the pre-fueling time.

These differences are the consequences of the combustion properties of hydrogen. In addition to its high reactivity, H_2-enrichment shifts the lean flammability limit ϕ_l toward lower equivalence ratios [21, 22]. As a result, ignition can occur in combustible air mixtures featuring a smaller equivalence ratio, i.e. a smaller fuel volume inside the chamber for mixtures with a high H_2-content compared to those with lower H_2 concentrations. This translates into lower reaction rates, leading to a smaller pressure perturbation inside the chamber. This is the predominant mechanism under ignition procedure A for which the total fuel mass inside the chamber at ignition has not yet reached the targeted value $Y_F^* << 1$. In these conditions, the fuel cannot perfectly mixed with the surrounding air already inside the combustion chamber, and a stratification of ϕ along the chamber length l_{cc} is expected. In a similar way, these effects are expected to be insignificant for a perfectly premixed volume in which case the equivalence ratio ϕ is homogeneous inside the chamber.

3.2.2 Ignition time delay

To further assess the impact of hydrogen enrichment on the amplitude of the pressure overshoot, two specific operating conditions are considered. They correspond to PH30 and PH70 flames at $\phi = 0.6$. Despite their large difference in terms of laminar burning velocity, $S_l^0 = 0.2$ m.s^{-1} for PH30 and 0.5 m.s^{-1} for PH70, Fig. 5.a shows that for ignition procedure A, both conditions achieve relatively the same pressure peak $p_{max} \sim 3$ kPa inside the chamber. In order to shed light on the physics controlling these similar over pressures, the total fuel mass inside the chamber at ignition should be compared. This quantity being difficult to measure experimentally, the total fuel mass flowrate $\dot{m}_f$ of methane and hydrogen is used instead. Qualitatively, this offers an acceptable approximation of the time evolution of Y_F^* inside the combustion chamber during pre-fueling. Time-series of the normalized chamber pressure (black solid line) as well as the normalized fuel mass flowrate are presented in Fig. 6 for both operating conditions considered in this section. The instant $t = 0$ s marks the fuel valve opening and the pressure peak is used to capture the ignition. The fuel mass flowrate signal is read from the MFCs.

Before exploiting the data, the dynamic response of the MFCs as well as their accuracy were verified under a wide range of operating conditions, starting from low pressure overshoot (100 Pa) up to 2×10^4 Pa. As they are placed far upstream of the burner at about ~ 4 m, the output of the MFCs remains unaffected by the ignition transient pressure perturbation no matter its magnitude as it can be seen in Fig. 6. Observation suggests that the pressure wave is dumped/reflected in the pipes.

To achieve a consistent comparison of the ignition time delay τ_{ign}, defined as the time difference between the fuel valve opening and the appearance of the first flame branch, the resi-

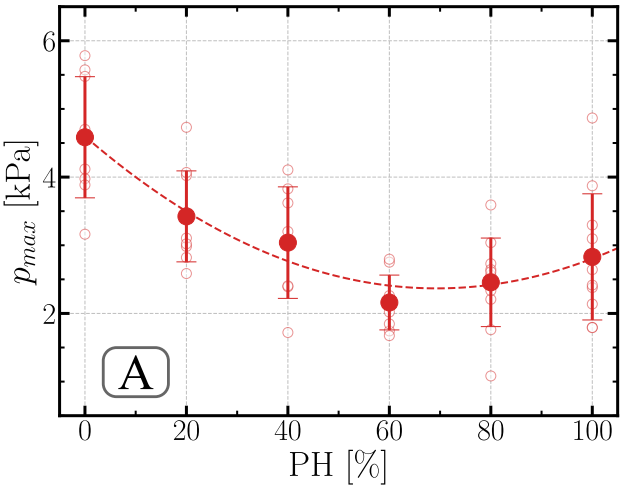

Fig. 8: Magnitude of the pressure overshoot reached during ignition for the operating conditions given in Tab. 1 for ignition procedure A.

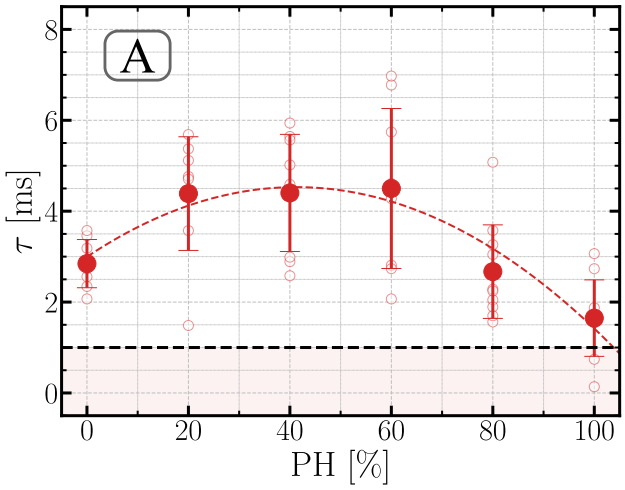

Fig. 9: Time lag τ between the chamber pressure and OH^* peak intensity for the operating conditions given in Tab. 1. The black dashed line marks $\tau_c = 1$ ms.

dence time inside the pipes $t_{res} \sim 0.6$ s is subtracted from the time reference corresponding to the mass flowrate signal. It is also worth mentioning that since the spark plug mean energy is two order of magnitude higher than the minimum ignition energy, τ_{ign} is uniquely determined by the mixture composition at ignition.

Figure 6 clearly shows that ignition occurs much earlier for the PH70 flame with $\tau_{ign} \sim 0.15$ s while PH30 flame ignites only after $\tau_{ign} \sim 0.5$ s. In other words, the total fuel amount inside the chamber at ignition is smaller for the PH70 flame compared to the PH30 case due to the extension of the lower flammability limit for the PH70 case. In fact τ_{ign} marks the fuel injection time before ignition, therefore, as τ_{ign} goes to zero, the instantaneous equivalence ratio at ignition tends to the one corresponding to the lean flammability limit. On the other hand, when τ_{ign} is larger, the instantaneous equivalence ratio at ignition tends to the targeted value.

These results are supported by Fig. 7 which plots the evolution of the ignition time delay τ_{ign} with respect to the H_2-content in the mixture for $\phi = 0.6$. This figure clearly shows that τ_{ign} quickly drops as the level of hydrogen enrichment increases when ignition procedure A is selected. For low H_2 concentrations, the fuel needs to be injected for a longer time in order to reach a sufficiently flammable mixture inside the combustion chamber. For high H_2-content in the mixture, the flammability limit is reached earlier. In the case of ignition procedure A, the high reactivity of hydrogen is compensated by the shift of the flammability limit ϕ_l towards lower equivalence ratios, which results in lower reaction rates.

Conversely, when ignition procedure B1 is used with $dt =$ 1 s, the ignition time delay for the PH10 flame is similar to the one observed for ignition procedure A ($\tau_{ign} \sim 0.8$ s). This indicates that at 10% H_2-content, the fuel needs to be injected at least for 0.8 s in order to reach a sufficiently flammable mixture. On the other hand, when PH exceed 20%, τ_{ign} remains relatively constant around $\tau_{ign} \sim 0.4 \pm 0.1$ s regardless the hydrogen enrichment. This value corresponds to the time difference with the pre-fuelling time from which the residence time t_{res} is subtracted: $dt - t_{res} = 0.4$ s. For the late ignition procedures B, the ignition time delay is set to be at least equal to the initial pre-fuelling time. In these conditions, the mixture inside the combustion chamber has already exceeded its flammability limit, causing an immediate ignition directly after the first spark.

By repeating the same analysis for ignition procedure B3 (not shown here), the same ignition time delay $\tau_{ign} \sim 2.6 \pm 0.1$ s is found for all different flames. Again, this value corresponds to $dt - t_{res}$ which in this case is equal to 2.6 s. With this pre-fuelling time lag, all the combustible mixture has already exceeded the flammability limit, and the only dominant effect due to hydrogen enrichment is its high reactivity. This result confirms the previous analysis suggesting that variations in terms of flammability limits on the ignition dynamics become less significant as the pre-fueling time dt increases.

4 Ignition dynamics at constant bulk flow velocity and constant burning velocity

In the remainder, additional experiments at fixed injection velocity $U_b = 5$ m.s^{-1} and fixed laminar burning velocity $S_l^0 = 0.25$ m.s^{-1} are carried out for increasing H_2-contents (see Tab. 1). These operating conditions offer the possibility to partially isolate the flow dynamics from the effects of the combus-

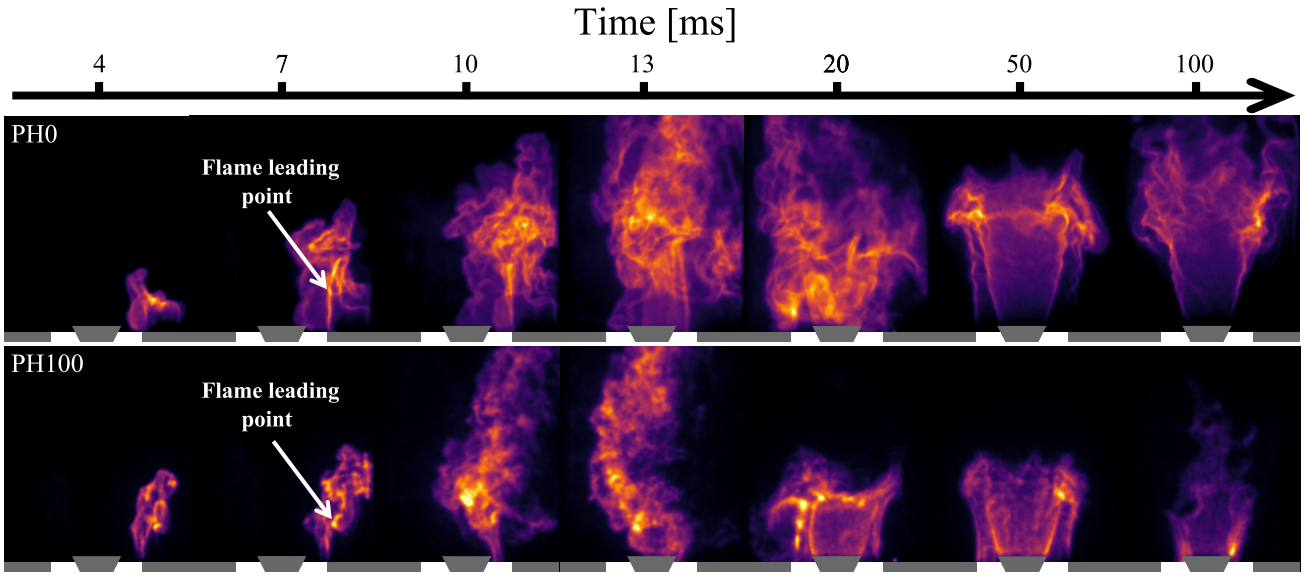

Fig. 10: Instantaneous OH* snapshots showing the ignition sequence from kernel formation to final stabilization for PH0 (top row) and PH100 (bottom row) with ignition procedure A.

tion properties of hydrogen [17]. In addition, keeping the laminar burning velocity S_l^0 constant enables to considerably mitigate the impact of the flame acceleration on the results. Ignition experiments are repeated eight to ten times to verify the repeatability of each sequence and allow accurate statistical measurements. In fully premixed conditions, it was shown that the enhanced reactivity of hydrogen reduces the time-lag between the pressure and the heat release rate peaks, therefore, promoting flashback [17]. The following section further explores the impact of the ignition procedure on both the final state and the aforementioned synchronisation condition for the early (procedure A) and late (procedure B) ignition procedures.

Table 1: Operating conditions at $U_b = 5$ m.s^{-1} and $S_l^0 = 0.25$ m.s^{-1} for six different levels of H_2-enrichment.

Cases	ϕ	$\mathcal{P}_{CH_4}$	$\mathcal{P}_{H_2}$	T$_{ad}$ [K]	$\mathcal{P}$ [kW]
PH0	0.78	100%	0%	1980	8.4
PH20	0.68	80%	20%	1850	7.6
PH40	0.60	60%	40%	1740	6.9
PH60	0.53	40%	60%	1630	6.3
PH80	0.48	20%	80%	1580	6.0
PH100	0.43	0%	100%	1500	5.7

4.1 Early ignition procedure: A

To keep the laminar burning velocity S_L^o constant, the equivalence ratio of the combustible mixture is reduced as the hydrogen content increases. Figure 8 shows the magnitude of the pressure overshoot reached with ignition procedure A for the six levels of hydrogen enrichment presented in Tab. 1. The maximum is reached for pure methane injection where it peaks at 4.5 kPa on average. As the hydrogen enrichment increases, p_{max} decreases reaching a minimum $p_{max} \sim 2.5$ kPa at PH60, before slightly increasing again up to $p_{max} \sim 3$ kPa for pure hydrogen injection.

As already discussed in the previous section, this behavior results from the competition of the total fuel mass inside the chamber at ignition and the broadening of the flammability limit towards lower equivalence ratios as the hydrogen concentration increases in the combustible mixture. For PH0 to PH60, the

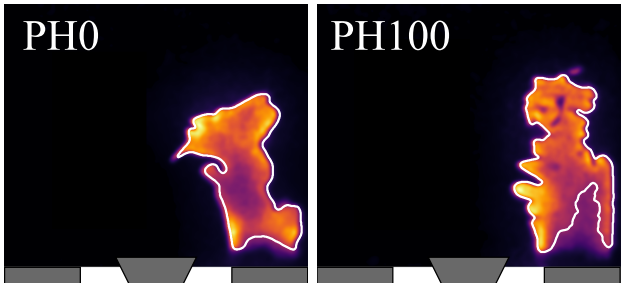

Fig. 11: Comparison of single-shot OH-PLIF at $t = 7$ ms for pure CH_4-air and H_2-air flame at fixed S_l^0. Ignition procedure A.

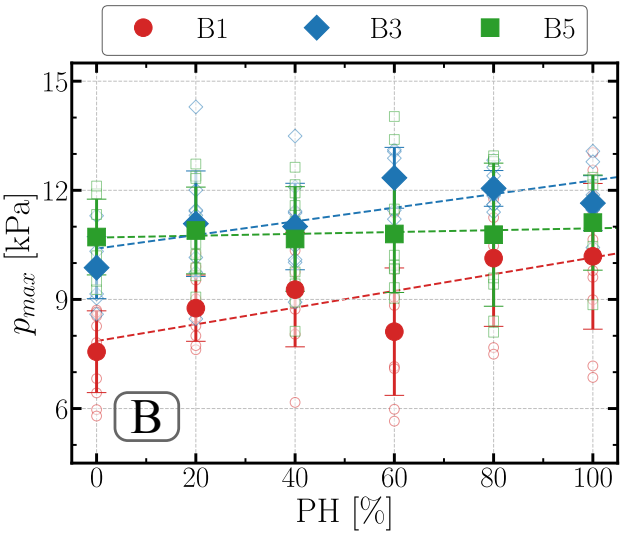

Fig. 12: Magnitude of the ignition overshoot for the operating conditions given in Tab. 1 using ignition procedures B1, B3 and B5.

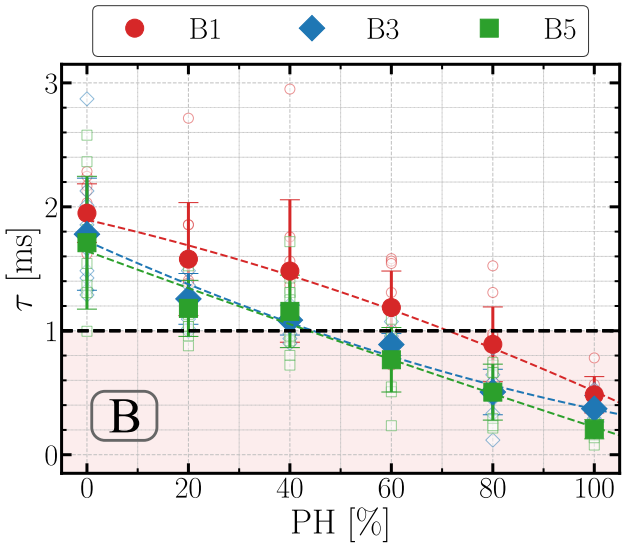

Fig. 13: Time lag between the chamber pressure and light intensity peaks for operating conditions given in Tab. 1. The black dashed line marks $\tau_c = 1$ ms.

higher flammability of the combustible mixture enables to ignite less fuel leading to a reduced pressure peak, but these experiments also show that the pressure impulse is less sensitive to changes of the flammability limit when the H_2-content exceeds 60% of the total thermal power. Indeed, at this level of hydrogen enrichment, preferential diffusion effects become significant given the lean conditions investigated ($\phi \leq 0.53$). Lean hydrogen mixtures featuring a Lewis number lower than unity, the flame speed S_d exceeds the laminar burning velocity S_l^0 due to the imbalance between heat and species diffusion leading to intrinsic reaction layer instabilities [23]. These thermo-diffusives effects contribute to further accelerate the flame front propagation counteracting the effects related to a lower flammability limit that tends to slow down flame propagation.

One now considers the time lag τ defined as the time difference between the peak pressure and the maximum heat release rate. It was shown in [17] that small τ values lead to flashback when the chamber is filled with an homogeneous combustible mixture at ignition. Conversely, when τ is sufficiently large, flashback is avoided. For the same operating conditions, a critical threshold value of $\tau_c \sim 1$ ms was found in [17] above which the flashback is avoided. Figure 9 shows how τ evolves with H2-enrichment. Up to 80% H_2-content, τ exceeds the threshold $\tau_c \sim 1$ ms leading to a soft ignition scenario in which case, all flames regardless the hydrogen enrichment level, directly stabilize on the bluff-body. For pure hydrogen injection PH100, the average time lag τ is of the order of magnitude of the critical threshold value $\tau \sim \tau_c$, meaning that some of the ignition sequences have $\tau < \tau_c$. It was indeed observed for these cases that the final state varies from an ignition sequence to another.

The dynamics of the traveling flame front from kernel formation to final stabilization is now investigated. Line-of-sight (LOS) integrated OH^* images are shown in Fig. 10 for pure methane (PH0) and pure hydrogen (PH100) injection. During the first instants of the ignition process $t \leq 10$ ms, both flames feature a peak intensity along the outer shear layer of the annular jet exhausting from the burner. Simultaneously, a weaker light intensity is observed in the jet region between the inner an the outer shear layers. At $t \simeq 10$ ms, the largest OH^* signal for the CH_4-air flame remains essentially located in the upper part region of the outer recirculation zone. Concomitantly flame images also show a lower intensity close to the burner lips suggesting that the most of the combustion reaction takes place far from the injector. For the H_2-air flame (PH100) case, the maximum OH^* signal is located instead in the wake region downstream the bluff-body, thus igniting the entire inner recirculation zone.

The corresponding OH-Planar Laser Induced Fluorescence (OH-PLIF) images, along the axial plane, are shown in Fig. 11 approximately at $t \simeq 7$ ms after ignition. These additional data confirm that for both mixtures, the flame branch initiated in the outer recirculation cannot penetrate inside the exiting jet. Despite its high resistance to stretch, the flame leading point is quenched near the injector outlet where the local strain rate is high and the reactive front is convected downstream along the outer shear layer. This comes to confirm previous observations in [16] where it was demonstrated that the ability of the flame to propagate into the different regions of the flow is essentially driven by flame resistance to the stretch in the shear regions of the flow.

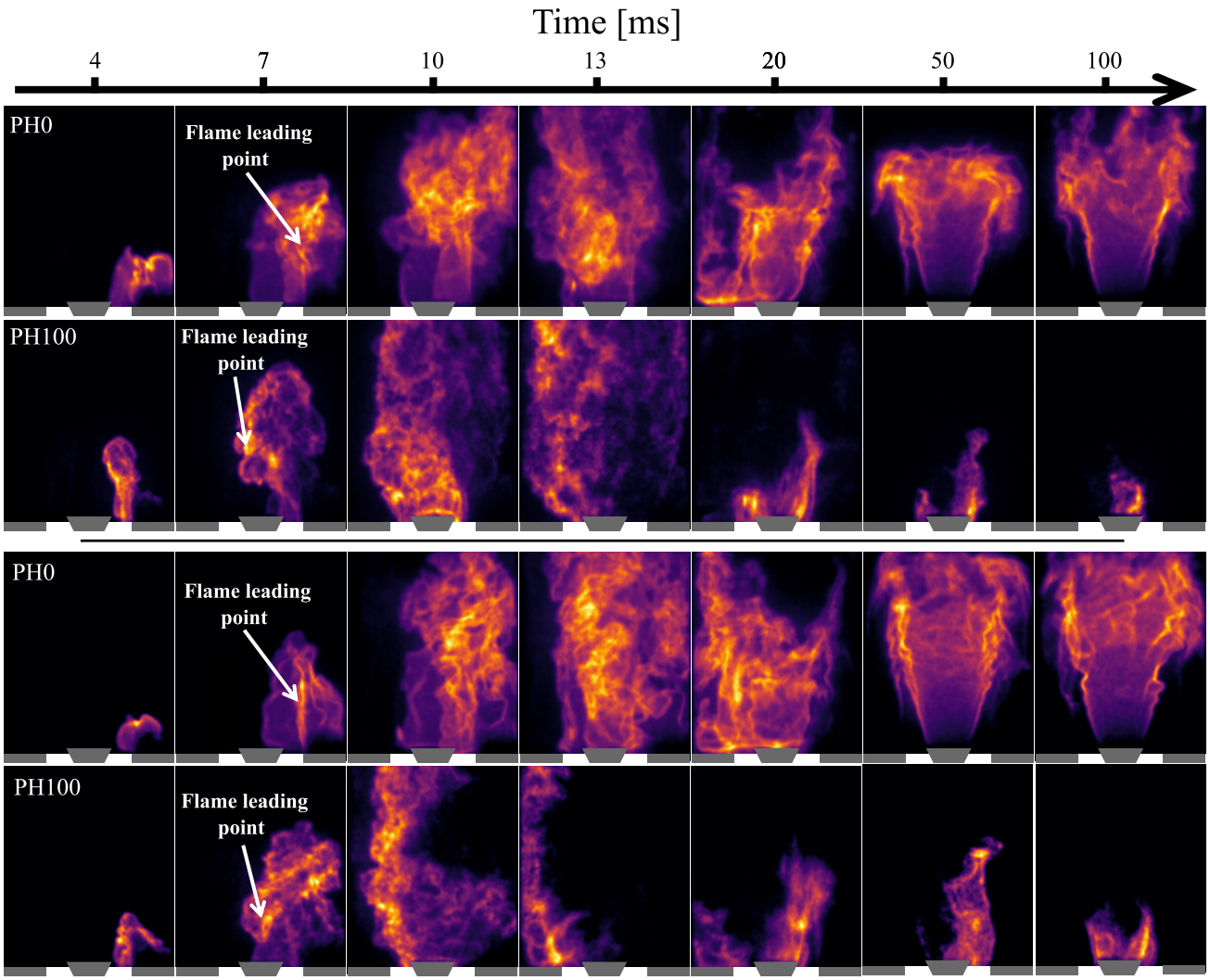

Fig. 14: Instantaneous OH^* snapshots showing the ignition sequence from kernel formation to final stabilization for PH0 and PH100 flames with ignition procedures B1 (two upper sequences) and B3 (two lower sequences).

4.2 Late ignition procedure: B

The previous experiments are repeated to examine changes when switching to ignition procedures B, all other parameters remaining the same, i.e. the impact of H2 enrichment is examined at fixed injection velocity and constant laminar burning velocity. Figure 12 shows the amplitude of the pressure peak recorded during ignition with respect to the hydrogen content in the fuel blend for procedures B1, B3 and B5. For ignition procedure B1, the absolute pressure peak p_{max} remains below the ones observed for procedures B3 and B5 over the entire span of mixtures. The lower magnitude p_{max} observed for the ignition procedure B1 is due to a smaller mass of fuel injected before ignition. Increasing the fuel delivery time to 3 s (B3) and 5 s (B5) promotes the formation of a larger premixed volume before ignition corresponding to Y_F^* values closer to unity. Burning of this larger fuel volume leads to a larger pressure peak. Figure 12 also shows that for ignition procedures B, the pressure peak p_{max} only slightly increases with the hydrogen concentration. For instance, in case of B1 p_{max} increases from 8 kPa at PH0 to 10 kPa at PH100, while for procedure B3 the pressure peak increases from 10 kPa at PH0 to 11.5 kPa at PH100. Relative variations are less than $\pm 20\%$. For ignition procedure B5, the pressure impulse varies by less than 10% over the entire span of H_2-enrichment. For this latter ignition procedure, the fuel delivery time is long enough to obtain a well premixed charge inside the combustion chamber, with a homogeneous mixture composition that corresponds

to the targeted equivalence ratio ϕ^{∞}. Under these conditions, the pressure peak p_{max} is not affected by the transient variation of the local mixture composition like for procedure B1 and B3. In addition, since the ratio of the bulk velocity to laminar burning velocity is kept constant, the amplitude of the over pressure does not change, corroborating previous observations obtained for a chamber filled with an homogeneous mixture [17].

The time lags τ measured between the pressure peak and the maximum heat release rate for ignition procedure B1, B3 and B5 procedure are reported in Fig. 13. In contrast to the results observed for ignition procedure A, the time lag τ reduces as the H_2-content in the mixture increases, recovering a similar trend as the one observed in [17] for a chamber filled with an homogeneous combustible mixture. Moreover, experiments also show that for a small pre-fuelling time with procedure B1, the time lag τ reaches slightly higher values compared to ignition strategies B3 and B5 with a longer pre-fuelling time. The critical hydrogen concentration above which the time lag τ drops bellow $\tau_c \sim 1$ ms is shifted towards lower H_2 concentrations as the pre-fuelling time dt increases. For instance, the transition from stable flame to flashback occurs for a hydrogen concentration larger than PH $\geq 80\%$ for ignition procedure B1, while this transition already takes place for mixtures at PH60 for procedure B3 and PH40 for procedure B5.

To further assess the impact of the pre-fuelling time on the final stabilization state, the dynamics of the traveling flame branch is explored with LOS-OH* images in Fig. 14. The top two rows correspond to results for procedure B1. The two bottom rows are obtained with procedure B3. For both procedures, the PH0 and PH100 cases are reported (See Tab.1). Similarly as with ignition procedure A, the CH_4-air flames follow a soft ignition scenario and directly stabilizes on the bluff-body, regardless the selected ignition procedure (B1 or B3). In these conditions, the time lag τ is higher than the 1 ms threshold in Fig. 9 and the maximum OH* intensity for $t \leq 10$ ms is essentially concentrated along the outer shear layer of the annular jet exhausting the burner. For the H_2-air flame PH100 in Fig. 14, the maximum light intensity during the same time interval is located in a region close to the wake of the bluff-body causing an immediate flashback just after ignition independently of the ignition procedure B1 or B3. In these cases, Fig. 13 confirm that the time lag τ takes values lower than 1 ms. These observations corroborate again the behavior observed in [17] where the flame was ignited 5 s after fuel injection corresponding to ignition procedure B5 in this study.

This analysis is supported by the instantaneous OH-PLIF images at $t \simeq 7$ ms shown in Fig. 15 for procedures B1 (top row) and B3 (bottom row), confirming that the trajectory of the flame leading edge after ignition highly differs between the PH0 and PH100 flames. For CH_4-air mixtures, the flame is quenched near the injector outlet, in correspondence of the high-strained region of the flow. In this case, the flame cannot penetrate inside the jet exhausting from the burner. The leading edge reaction layer is

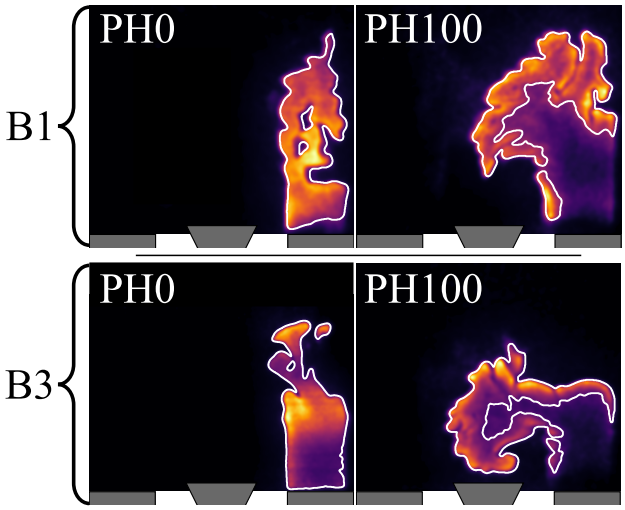

Fig. 15: Comparison of single-shot OH-PLIF at $t = 7$ ms for pure CH_4-air and H_2-air flame at fixed S_l^0 for ignition procedures B1 (top row) and B3 (bottom row).

advected downstream in the vertical direction. When methane is replaced by hydrogen, instead, the flame resistance to stretch improves and the flame front is able to propagate through the outer shear layer, quickly reaching the inner recirculation zone for both ignition procedures B1 and B3. This difference between methane and hydrogen mixtures is likely considered to be the cause of the several types of stabilization observed in this study.

In addition to flame resistance to stretch, preferential diffusion effects come to modify the local flame consumption speed. For lean hydrogen/air flames, intrinsic instabilities take the form of cellular structures leading to a substantial increase of flame front wrinkling [23, 24]. This increase in the total flame surface area (see Fig. 15) enhances the flame speed which may counterbalance the high shear strain region of the flow, hence, reducing the time lag τ between the pressure and light intensity peaks.

5 Conclusion

The impact of the ignition sequence on the ignition dynamics of CH_4-H_2-Air premixed flames has been investigated. Two main procedures were considered by varying the pre-fuelling time before ignition: (A) An early ignition procedure with the spark being first initiated before fuel injection. (B) Late ignition procedure where the fuel is first injected and then the spark is delayed with a time lag $dt = 1$, 3 and 5 s.

First, it has been shown that the final stabilization state is highly sensitive to the selected ignition strategy especially for mixtures with a high H_2-content. Even a small variation in the fuel delivery time, of the order of 1 s, can lead to a violent ignition where the magnitude of the pressure exceeds 30 kPa. As a consequence, the ignition time window leading to a safe ignition

process is drastically reduced when the H_2-content exceeds 40% of the total thermal power (PH $>$ 40). At constant power, it was found that despite the significant increase of the laminar burning velocity due to hydrogen enrichment, the pressure peak reached during ignition achieves approximately the same amplitude for concentrations $30 \leq \text{PH} \leq 70$ when procedure A is selected. This overpressure was found to be mainly driven by the competition between the total fuel mass injected at ignition and the high reactivity of hydrogen which tends to shift the lean flammability limit towards lower value of equivalence ratio.

Finally, for a fixed bulk flow velocity and a constant laminar burning velocity, the ignition procedure has been shown to substantially alter the ignition dynamics. The maximum pressure overshoot recorded with ignition procedure A remains below the over pressure observed for procedure B independently of the pre-fuelling time. Direct flame visualisation revealed that the trajectory of the flame leading point changes with both H_2-content and pre-fueling time. The ability of the flame to penetrate through the mixing layer of the exiting jet determines the final stabilisation mode. In the case of non-penetration due to high strain at the burner outer shear layer, the flame propagation is temporary slowed down as the reactive front is constrained to propagate axially downstream in the low strain region. This helps increasing the time lag τ between the pressure and heat release rate peaks preventing the flashback. Conversely, a quick flame penetration inside the premixed jet offers preferential conditions to trigger flashback. These differences in terms of flame leading point behaviour close to the injector rim, is found to be the cause of the different type of stabilization observed in this study.

Acknowledgements

This publication has been produced with support from the NCCS Centre, performed under the Norwegian research program Centres for Environment-friendly Energy Research (FME) (Grant 257579/E20).

REFERENCES

[1] Kakoulaki, G., Kougias, I., Taylor, N., Dolci, F., Moya, J., and Jäger-Waldau, A., 2021. "Green hydrogen in Europe–A regional assessment: Substituting existing production with electrolysis powered by renewables". *Energy Convers. Manag.,* ***228***, p. 113649.

[2] Capurso, T., Stefanizzi, M., Torresi, M., and Camporeale, S. M., 2022. "Perspective of the role of hydrogen in the 21st century energy transition". *Energy Convers. Manag.,* ***251***, p. 114898.

[3] Bothien, M. R., Ciani, A., Wood, J. P., and Fruechtel, G., 2019. "Toward decarbonized power generation with gas turbines by using sequential combustion for burning hydrogen". *J. Eng. Gas Turbines Power,* ***141***(12), p. 121013.

[4] Fischer, M., 1986. "Safety aspects of hydrogen combustion in hydrogen energy systems". *Int. J. Hydrogen Energy,* ***11***(9), pp. 593–601.

[5] Sánchez, A. L., and Williams, F. A., 2014. "Recent advances in understanding of flammability characteristics of hydrogen". *Prog. Energy Combust. Sci.,* ***41***, pp. 1–55.

[6] Neuman, J. A., 1908. "Electric ignition for gas engines". PhD thesis, University of Illinois, Chicago, USA.

[7] Lefebvre, A. H., and Ballal, D. R., 2010. *Gas turbine combustion: alternative fuels and emissions*. CRC press, doi.org/10.1201/9781420086058.

[8] Moorhouse, J., Williams, A., and Maddison, T. E., 1974. "An investigation of the minimum ignition energies of some C1 to C7 hydrocarbons". *Combust. Flame,* ***23***(2), pp. 203–213.

[9] Danis, A. M., Namer, I., and Cernansky, N. P., 1988. "Droplet size and equivalence ratio effects on spark ignition of monodisperse N-heptane and methanol sprays". *Combust. Flame,* ***74***(3), pp. 285–294.

[10] Wu, C., Chen, Y.-R., Schießl, R., Shy, S. S., and Maas, U., 2022. "Numerical and experimental studies on minimum ignition energies in primary reference fuel/air mixtures". *Proc. Combust. Inst.,* ***doi.org/10.1016/j.proci.2022.08.043***(In press).

[11] Mastorakos, E., 2009. "Ignition of turbulent non-premixed flames". *Prog. Energy Combust. Sci.,* ***35***(1), pp. 57–97.

[12] Cordier, M., Vandel, A., Cabot, G., Renou, B., and Boukhalfa, A. M., 2013. "Laser-induced spark ignition of premixed confined swirled flames". *Combust. Sci. Technol.,* ***185***(3), pp. 379–407.

[13] Ahmed, S. F., Balachandran, R., Marchione, T., and Mastorakos, E., 2007. "Spark ignition of turbulent nonpremixed bluff-body flames". *Combust. Flame,* ***151***(1-2), pp. 366–385.

[14] Bourgouin, J.-F., Durox, D., Schuller, T., Beaunier, J., and Candel, S., 2013. "Ignition dynamics of an annular combustor equipped with multiple swirling injectors". *Combust. Flame,* ***160***(8), pp. 1398–1413.

[15] Philip, M., Boileau, M., Vicquelin, R., Riber, E., Schmitt, T., Cuenot, B., Durox, D., and Candel, S., 2015. "Large Eddy Simulations of the ignition sequence of an annular multiple-injector combustor". *Proc. Combust. Inst.,* ***35***(3), pp. 3159–3166.

[16] Pouech, P., Duchaine, F., and Poinsot, T., 2021. "Premixed flame ignition in high-speed flows over a backward facing step". *Combust. Flame,* ***229***, p. 111398.

[17] Yahou, T., Dawson, J. R., and Schuller, T., 2022. "Impact of chamber back pressure on the ignition dynamics of hydrogen enriched premixed flames". *Proc. Combust. Inst.,* ***doi.org/10.1016/j.proci.2022.07.236***(In press).

[18] Prieur, K., Vignat, G., Durox, D., Schuller, T., and Candel, S., 2019. "Flame and spray dynamics during the light-

round process in an annular system equipped with multiple swirl spray injectors". *J. Eng. Gas Turbines Power,* ***141***(6).

[19] Töpperwien, K., Collin-Bastiani, F., Riber, E., Cuenot, B., Vignat, G., Prieur, K., Durox, D., Candel, S., and Vicquelin, R., 2021. "Large-eddy simulation of flame dynamics during the ignition of a swirling injector unit and comparison with experiments". *J. Eng. Gas Turbines Power,* ***143***(2).

[20] Philip, M., Boileau, M., Vicquelin, R., Schmitt, T., Durox, D., Bourgouin, J.-F., and Candel, S., 2015. "Simulation of the ignition process in an annular multiple-injector combustor and comparison with experiments". *J. Eng. Gas Turbines Power,* ***137***(3).

[21] Yu, G., Law, C. K., and Wu, C. K., 1986. "Laminar flame speeds of hydrocarbon+ air mixtures with hydrogen addition". *Combust. Flame,* ***63***(3), pp. 339–347.

[22] Eckart, S., Pizzuti, L., Fritsche, C., and Krause, H., 2022. "Experimental study and proposed power correlation for laminar burning velocity of hydrogen-diluted methane with respect to pressure and temperature variation". *Int. J. Hydrogen Energy,* ***47***(9), pp. 6334–6348.

[23] Berger, L., Attili, A., and Pitsch, H., 2022. "Intrinsic instabilities in premixed hydrogen flames: parametric variation of pressure, equivalence ratio, and temperature. Part 2–Non-linear regime and flame speed enhancement". *Combust. Flame,* ***240***, p. 111936.

[24] Berger, L., Attili, A., and Pitsch, H., 2022. "Synergistic interactions of thermodiffusive instabilities and turbulence in lean hydrogen flames". *Combust. Flame,* ***244***, p. 112254.